Extraction of Micro-Doppler Features from Unmanned Aerial Vehicles Based on Electromagnetic Simulation

Guohao Lu *, Zhongyuan Song

College Of Electronic and Information Engineering, Hebei University, Baoding, China, 071002

* Corresponding Author Email: guohao_lu@126.com

Abstract. With the rapid development of drone technology, the micro-Doppler signature plays a crucial role in the recognition and classification of drones. However, existing methods for extracting micro-Doppler signals are often affected by the complex structure of targets and environmental interferences, leading to issues of low extraction accuracy and efficiency. In response to this challenge, this paper investigates a method for extracting rotor micro-Doppler signals of Unmanned Aerial Vehicles (UAVs) based on electromagnetic simulation. By establishing the geometric model of the target object and using the physical optics method for RCS measurement of the model, the obtained data is utilized for inverse ISAR imaging to obtain the scattering center positions and scattering intensity of each point on the rotor. A model for extracting micro-Doppler properties is established, enabling accurate and efficient extraction of micro-Doppler characteristics for target objects. The proposed method can be widely applied to extract and study the micro-Doppler characteristics of different types of drones.

Keywords: Micro-Doppler Signature, Radar Cross Section (RCS), Inverse Synthetic Aperture Radar (ISAR), Unmanned Aerial Vehicles.

1. Introduction

In recent years, with the continuous expansion of drone applications, the use of radar for identifying and classifying drones has become a focal point of research. Currently, extracting and analyzing the micro-Doppler characteristics of drones has become the primary method for their identification and classification [1-5]. Therefore, studying how to efficiently and accurately obtain the micro-Doppler characteristics of drones is of significant importance.

Currently, there are two main methods for extracting micro-Doppler signature from drones based on the echo data obtained. The first method is entirely based on signal-level simulation, where echo data is obtained by autonomously setting parameters such as scattering center positions and RCS under radar simulation, and then micro-Doppler characteristics are extracted [6]. The other method involves detecting actual objects with radar to obtain echo data, followed by micro-Doppler signal extraction [7].

If the target or any structure on the target has mechanical vibration or rotation in addition to its bulk translation, it might induce a frequency modulation on the returned signal that generates sidebands about the target's Doppler frequency shift. This is called the micro-Doppler effect [8]. The micro-Doppler effect in UAVs predominantly stems from the rotor. In the case of multirotor drones, the unique initial rotational phase of each rotor obscures the clear display of periodic Doppler modulation in the combined micro-Doppler characteristics [7]. This paper primarily explores the extraction of micro-Doppler signals from UAVs based on electromagnetic simulation, simplifying the approach by focusing on extracting signals from a single rotor of a drone.

The study commences by establishing a model of a three-blade rotor using electromagnetic simulation techniques, specifically employing physical optics to determine the rotor's RCS. Subsequently, the acquired RCS data undergoes processing via ISAR to derive the positions of scattering centers and their respective intensities on the rotor. Utilizing this information, each point is subjected to rotation at specific speeds to simulate the rotor's rotational behavior. Under the simulated radar environment, the resulting echo data during rotor rotation is obtained. Finally, the

micro-Doppler characteristics of the rotor are derived through a Short-Time Fourier Transform (STFT).

This approach, which establishes an authentic rotor model and acquires data on scattering centers and intensities through electromagnetic simulation, presents a more realistic alternative to micro-Doppler models established by independently configuring scattering center and intensity parameters. Moreover, the extracted micro-Doppler characteristics not only exhibit enhanced realism and precision but also offer greater efficiency and resource conservation compared to direct measurement approaches.

2. Algorithm Principle

2.1. Definition of RCS

An object exposed to an electromagnetic wave disperses incident energy in all directions. This spatial distribution of energy is called scattering, and the object itself is often called a scatterer. The energy scattered back to the source of the wave (called backscattering) constitutes the radar echo of the object. The intensity of the echo is described explicitly by the radar cross-section of the object, for which the abbreviation RCS has been generally recognized [8]. RCS can be defined by the following equation [9].

$$\sigma = \lim_{R \to \infty} 4\pi R^2 \frac{|E_s|^2}{|E_0|^2} \tag{1}$$

The RCS computations in this paper were conducted using the FEKO simulation software with the Physical Optics (PO) method. However, we do not provide a detailed derivation of the PO method in this paper. For further information on RCS computation using the PO method, please refer to [10].

2.2. Principle of ISAR

An ISAR image is formed by coherently processing a returned signal from a moving target at a different aspect angle relative to the radar. The change of the aspect angle is usually due to relative motion and rotation between the radar and the target. When the target is moving smoothly, conventional motion compensation algorithms that correct for any changes in the target's velocity vector can be applied to generate a clear image of the target [11]. ISAR can be classified into single-baseline ISAR and dual-baseline ISAR. In single-baseline ISAR, radar transmission and reception occur at the same position, whereas in dual-baseline ISAR, they occur at different positions. This study employs the single-baseline ISAR configuration. Generating ISAR images involves capturing echo signals at various angles and frequencies, followed by processing to produce the final ISAR images.

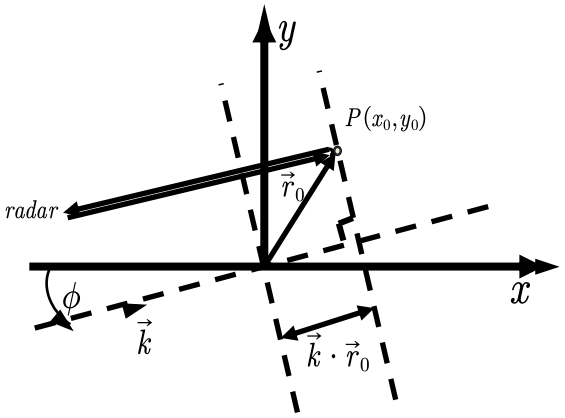

Figure 1. Translation of Radar and Rotor Relative Position Diagram

As illustrated in Figure 1, suppose there is a scattering center $P(x_0, y_0)$ on the rotor. When its azimuth angle is ϕ, i.e., when the wave vector $\vec{k}$ forms an angle of ϕ with the x-axis, $\vec{r_0}$ represents the vector pointing from the origin to point P. The magnitude of the backscattered field at point P is approximately.

$$E^s(k,\phi) \cong A_0 \cdot e^{-j2\vec{k}\cdot\vec{r}_0} \tag{2}$$

Where A_0 represents the magnitude of the backscattered field at the scattering center, where $e^{-j2\vec{k}\cdot\vec{r}_0}$ is the phase term. By expressing $\vec{k}$ and $\vec{r}_0$ using unit direction vectors along the x and y axes, respectively, we obtain the following equation.

$$\begin{cases} \vec{r} = x_0 \cdot \hat{x} + y_0 \cdot \hat{y} \\ \vec{k} = |k| \cdot \cos\phi \cdot \hat{x} + |k| \cdot \sin\phi \cdot \hat{y} \end{cases} \tag{3}$$

Substituting Equation (3) into Equation (2), we obtain.

$$E^s(k,\phi) = A_0 \cdot e^{-j2k\cos\phi \cdot x_0} \cdot e^{-j2k\sin\phi \cdot y_0} \tag{4}$$

Where k represents the wave number at a signal frequency of f.

$$k = \frac{2\pi f}{c} \tag{5}$$

The equation encompasses two phase terms, $e^{-j2k\cos\phi \cdot x_0}$ and $e^{-j2k\sin\phi \cdot y_0}$, and it is evident that these two phase terms are each related to x and y through Fourier transformation. Consequently, the two-dimensional ISAR image can be obtained through a two-dimensional inverse Fourier transform of the backscattered field from the scattering centers.

In most practical radar applications, the conditions adhere to the small-angle ISAR imaging. The radar bandwidth B is much smaller compared to the center frequency of the transmitted signal f_c. Therefore, in Equation (4), the k term in the second phase term can be approximated as k_c, k_c represents the wave number at f_c.

When the imaging angle ϕ is less than 5 or 6 degrees, it is considered to be small-angle imaging. In this case, ϕ can be approximated as follows.

$$\begin{cases} \cos\phi \cong 1 \\ \sin\phi \cong \phi \end{cases} \tag{6}$$

Substituting Equation (6) into Equation (4).

$$E^s(k,\phi) = A_0 \cdot e^{-j2\pi\left(\frac{2f}{c}\right)x_0} \cdot e^{-j2\pi\phi\left(\frac{2f_c}{c}\right)\cdot y_0} \tag{7}$$

Performing a two-dimensional inverse Fourier transform on the above equation yields the two-dimensional ISAR image.

$$F_2^{-1}\{E^s(k,\phi)\} = A_0 \cdot F\left\{e^{-j2\pi\left(\frac{2f}{c}\right)x_0}\right\} \cdot F_1^{-1}\left\{e^{-j2\pi\left(\frac{k_c\phi}{\pi}\right)\cdot y_0}\right\} \tag{8}$$

$$\begin{aligned} E^s(x,y) &= A_0 \cdot \left[\int_{-\infty}^{\infty} e^{-j2\pi\left(\frac{2f}{c}\right)\cdot x_0} \cdot e^{j2\pi\left(\frac{2f}{c}\right)\cdot x} d\left(\frac{2f}{c}\right) \right] \\ &\quad \cdot \left[\int_{-\infty}^{\infty} e^{-j2\pi\left(\frac{k_c\phi}{\pi}\right)\cdot y_0} e^{j2\pi\left(\frac{k_c\phi}{\pi}\right)\cdot y} d\left(\frac{k_c\phi}{\pi}\right) \right] \\ &= A_0 \cdot \delta(x - x_0, y - y_0) \\ &= ISAR(x,y) \end{aligned} \tag{9}$$

The final ISAR image represents the electromagnetic scattering distribution of multiple scattering centers.

2.3. The principle of micro-Doppler feature extraction

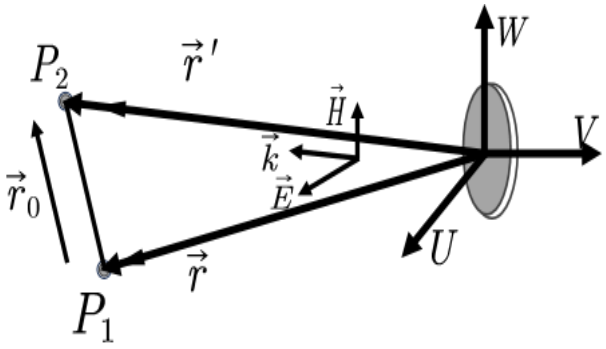

Figure 2. Translation of Rotor Before and After Translation Position Diagram

As illustrated in Figure 2, where P_1 and P_2 respectively represent the coordinates before and after the object's movement, the far-field electric field of a moving target can be defined as [12].

$$\vec{E}_T(\vec{r}\,') = \exp\{jk\vec{r}_0 \cdot (\vec{u}_k - \vec{u}_r)\}\vec{E}(\vec{r}) \tag{10}$$

Where, k represents the wave number, $\vec{r}$ and $\vec{r}\,'$ denote the vectors from the radar coordinate origin to points P_1 and P_2, respectively. $\vec{u}_k$ represents the unit vector of the incident wave, $\vec{u}_r$ represents the unit vector in the observation direction, $\vec{r}_0$ denotes the vector pointing from P_1 to P_2, which is the translational vector of the moving target, $\vec{r}_0 = \vec{r}\,' - \vec{r}$.

It can be observed that the far electric field changes solely in the phase term during the target's movement. When $\vec{r}_0$ is a function of time.

$$\vec{r}_0(t) = r_0(t)\,\vec{u}_T \tag{11}$$

Where $\vec{u}_r$ representing the unit translational vector

In the case of reverse scattering, where the observation direction is opposite to the incident direction.

$$\vec{u}_k = -\vec{u}_r \tag{12}$$

Substituting Equations (11) and (12) into Equation (10), we obtain.

$$\vec{E}_T(\vec{r}\,') = \exp\{2jkr_0(t) \cdot \vec{u}_T \cdot \vec{u}_k\}\vec{E}(\vec{r}) \tag{13}$$

When the radar emits electromagnetic waves at frequency f , the received signal can be represented as [12].

$$s(t) = \exp\{j2kr_0(t)\vec{u}_T \cdot \vec{u}_k\}\exp\{-j2\pi ft\}\left|\vec{E}(\vec{r})\right| \tag{14}$$

The change caused by the motion $\vec{r}_0(t)$ is defined as the micro-Doppler modulation effect, which occurs solely in the phase term. Doppler frequency shift can be expressed as follows [12].

$$f_D = \frac{2f}{c}\left[\vec{V} + \vec{\omega} \times \vec{r}'\right]_{radial} \tag{15}$$

The first term represents the Doppler shift caused by translation, while the second term accounts for the micro-Doppler modulation effect induced by rotation. Therefore, the micro-Doppler modulation effect ultimately manifests as a variation in frequency over time.

The micro-Doppler effect can be observed through the deviation of the spectrum from the central frequency. Joint time-frequency analysis is used for analyzing the time-dependent spectral content of micro-Doppler signals. It can be applied to mono-component as well as multi-component signals. Its techniques are classified into linear time-frequency transforms and bilinear time-frequency transforms [1]. Among the commonly used linear time-frequency transforms is the short-time Fourier transform. This paper employs time-domain analysis to investigate the relationship between the spectrum and time in the micro-Doppler modulation effect generated by rotor rotation. Using the short-time Fourier transform ultimately yields the micro-Doppler frequency. The expression for the short-time Fourier transform is as follows.

$$S(\tau, w) = \int_{-\infty}^{\infty} s(t)w(t-\tau)\exp(-jwt)dt \tag{16}$$

In the above equation, $s(t)$ represents the radar's received echo signal, and $w(t-\tau)$ denotes the window function applied to the time-domain signal. After performing the short-time Fourier transform, the relationship between the original signal in the time domain and its representation in the frequency domain can effectively capture the micro-Doppler modulation effect.

3. Results

3.1. RCS Simulation Results

This paper investigates a rot1or model of an Unmanned Aerial Vehicle (UAV) and employs the physical optics method in FEKO to compute its RCS. The radar's incident wave is characterized by a central frequency of 3 GHz, with a start frequency of 2.606 GHz and an end frequency of 3.417 GHz. The frequency increment is set to 45.1 MHz, with a total of 19 frequency samples. The azimuth angle spans from -8.61° to 8.61° with an angular interval of 0.956°, resulting in 19 azimuth directions. Linear polarization is utilized. The three-dimensional geometric model of the rotor's RCS is depicted in Figure 3. The results of computing the field in the direction of plane wave incidence under far-field single-station RCS are presented in the figure.

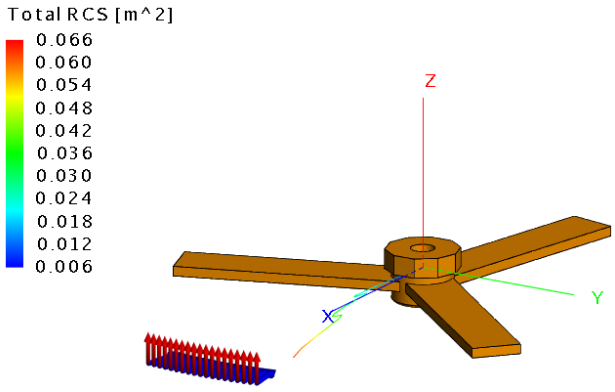

Figure 3. RCS Radar Observation Angle Diagram

Compute the field in the direction of plane wave incidence under far-field single-station RCS, and represent the results using Cartesian coordinates in FEKO as shown in Figure 4.

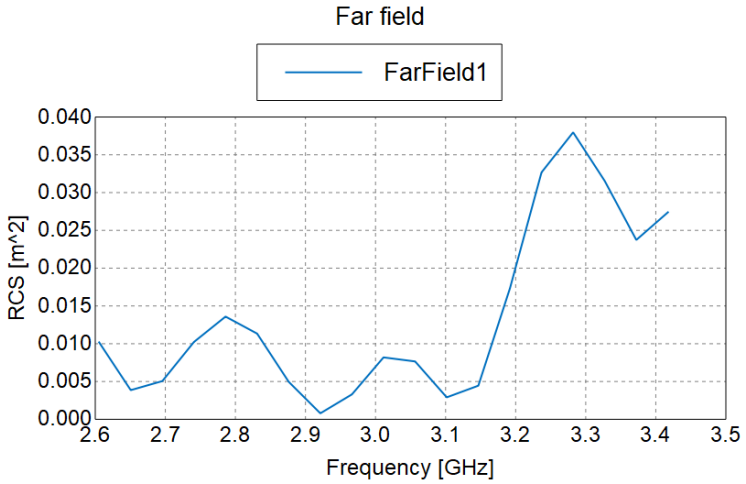

Figure 4. RCS vs. Frequency Variation Relationship Diagram

The horizontal and vertical axes of Figure 4 represent frequency and RCS, respectively. The horizontal axis ranges from the starting frequency to the stop frequency, while the RCS exhibits varying changes correspondingly. There are a total of 19 frequency samples, each indicating different reflection intensities of the rotor under different frequency excitations in the far-field conditions. The obtained RCS data will be further utilized for rotor ISAR analysis.

3.2. ISAR Simulation Results

The ISAR image provides a two-dimensional distribution of the target's main scattering centers, including their geometric positions and radar cross-sections [13].

In the ISAR simulation, the Hamming Window is set as the window function, with a viewing angle of -6.93E-14° and a viewing angle range of 17.218°. The ISAR image generated in FEKO is depicted in the figure.

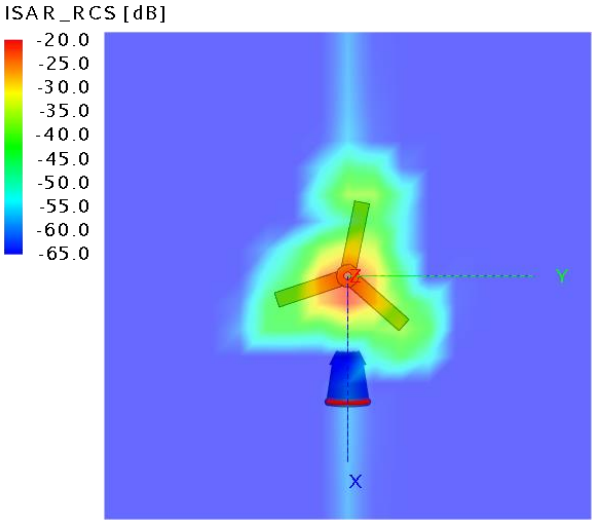

Figure 5. ISAR Imaging Results

From Figure 5, it can be observed that although there are variations in the reflection intensity of different parts of the rotor in the ISAR imaging, the reflected radar image generally conforms to the shape of the rotor blades. The reflection signals are distributed around the three rotor blades. The ISAR-generated data can be displayed in POSTFEKO using a standard Cartesian coordinate system [14], as shown in Figure 6.

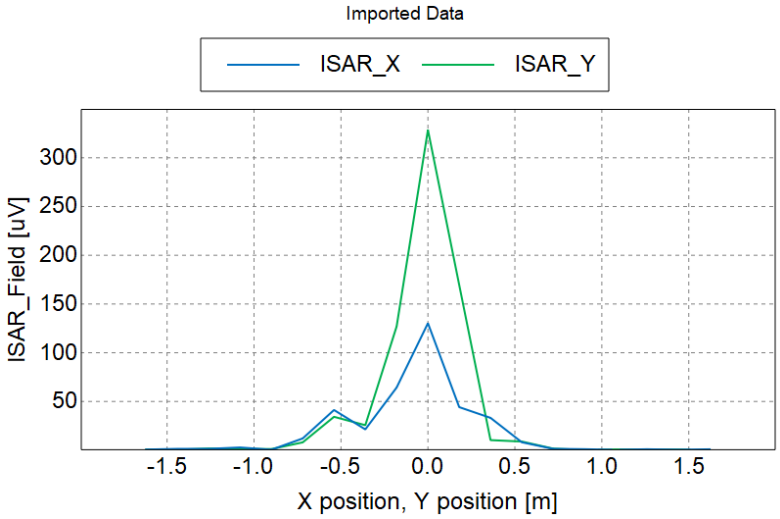

Figure 6. ISAR Imaging Results Coordinate Diagram

The ISAR field intensity, as depicted in Figure 6, exhibits a predominant concentration in the X-direction between -0.6 and 0.4, reaching a peak value of 125. Similarly, in the Y-direction, the intensity is concentrated primarily between -0.5 and 0.4, with a peak value of 325.

This substantiates the validity of the experiment and underscores the feasibility of the ISAR data. Furthermore, it underscores the potential applicability of ISAR-generated data in subsequent Doppler transformations.

3.3. Micro-Doppler Feature Extraction

3.3.1Data Processing

The data required for micro-Doppler feature extraction includes the coordinates distribution of different scattering centers obtained from the previous ISAR simulation step, along with their corresponding scattering intensities. Utilizing FEKO for ISAR simulations on the rotor, we established a direct correlation between scatter center positions and their corresponding intensities. However, the scatter points obtained contain not only coordinates of various rotor points but also include data from other points within the ISAR imaging range, extending beyond the rotor.

Since our experiment specifically focuses on extracting micro-Doppler features from scatter center positions and intensities exclusively associated with the rotor, it's crucial to eliminate extraneous information. Through observation, it was noted that the scattering intensity of points on the rotor is significantly higher than that of other scattering centers in the X, Y, Z, and RCS data obtained from the ISAR simulation. Therefore, scattering centers with relatively low intensity are not located on the rotor. Additionally, considering the rotor length is 0.5 meters, scattering centers with absolute X-coordinate values greater than 0.5 meters are also not on the rotor. Based on these observations, a threshold for scattering intensity of 1E-5 and an X-coordinate threshold of 0.5 meters were established. Consequently, points with scattering intensity less than 1E-5 and absolute X-coordinate values greater than 0.5 meters were filtered out. After this filtering process, 26 sets of scattering center data with corresponding intensity were obtained for micro-Doppler feature extraction.

3.3.2 Establishment of UAVs Rotor Motion Model

Using the distributed data of scattering centers obtained from ISAR simulation, we establish a motion model for the drone rotor. In this paper, the motion of the UAVs rotor is composed of translational and rotational components, as depicted in Figure 7. The radar is located at the origin coordinates (0, 0, 0), while the initial position of the rotor is at point Q (500, 0, 100). The translational velocity of the rotor is (30, 0, 0), indicating movement along the x axis at a rate of 30 units per second. The rotational speeds of the rotor are set to $10 rad/s$, $40 rad/s$ and $100 rad/s$.

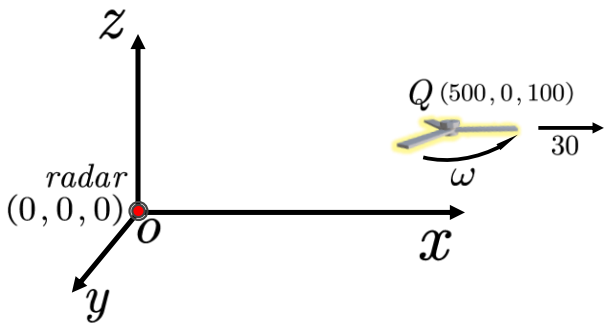

Figure 7. Rotor Rotation and Translation Illustration

The radar emits a periodic rectangular pulse wave as the transmission signal, with the following parameters: $speed$ representing the rotor speed, fs denoting the sampling rate of the transmission signal, PRF representing the pulse repetition frequency, and t indicating the duration of signal transmission. The setting of radar transmission signal parameters is shown in Table 1.

Table 1. Translation of Radar Transmission Signal Parameters Setting

speed(rad/s)	Pulse Width(us)	fs(kHz)	PRF(kHz)	t(s)
10	2	600	3	1
40	2	600	25	0.2
100	2	600	30	0.2

Using the scattering intensity data obtained from the aforementioned ISAR simulation, we establish a signal reflection model. In this model, the RCS represents the ISAR-RCS of each scattering center obtained from ISAR simulation. The carrier frequency of the reflected signal is set to 4GHz. After matching filtering of the obtained echo signals, a short-time Fourier transform is performed to observe the micro-Doppler modulation effect.

3.3.3 Results Analysis

The final time-domain distribution of the echo signals under three different rotational speeds (10 rad/s, 40rad/s, and 100rad/s) is depicted in Figures 8, respectively.

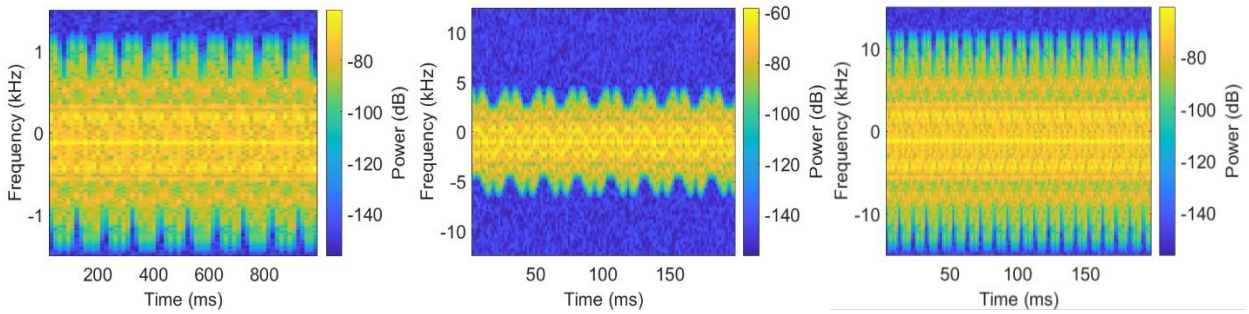

Figure 8. Time-Frequency Analysis Plots for Speeds 10rad/s, 40rad/s, and 100rad/s

For unmanned aerial vehicles, the rotating blades of the rotor can periodically modulate the Doppler frequency caused by the volume motion of the UAVs. Therefore, UAVs exhibit a unique characteristic of periodic time-varying Doppler frequency modulation, known as the micro-Doppler feature [15]. From the time-frequency plots, it can be observed that the frequency varies sinusoidally over time, consistent with the micro-Doppler modulation effect. It can be seen that when the rotor speeds are 10rad/s, 40rad/s, and 100rad/s, the corresponding Doppler frequency shifts are approximately 2.7 kHz, 11 kHz, and 27 kHz, respectively. According to the formula (15), the Doppler frequency shift range generated by different speeds should roughly be proportional to their speeds. The data obtained from the simulation conforms to theoretical expectations.

Furthermore, considering a rotor length of $0.5m$, and neglecting rotor translational motion, the theoretical range of micro-Doppler frequencies is approximately 1.7 kHz. Upon including translational motion, the theoretical range of micro-Doppler frequencies matches closely with the actual values obtained from the simulation.

4. Conclusion

This paper proposes a methodology for extracting micro-Doppler features from UAVs rotor motion using electromagnetic simulation. Initially, we constructed a model of the UAVs rotor. We then utilize data on scatter center positions and intensities obtained from RCS and ISAR simulations to parameterize the rotor. Subsequently, we establish a physical model of the rotor in motion based on this data. Radar simulations are conducted on the moving rotor model to gather echo data, which is analyzed using a short-time Fourier transform to extract micro-Doppler features. Experimental analysis validates our approach.

(1) The ISAR images closely resemble the shape of the UAVs rotor model, which is reasonable.

(2) Time-frequency analysis plots of the rotor exhibit periodic sinusoidal patterns, characteristic of micro-Doppler effects.

(3) Increasing rotor speeds lead to stronger target echoes and more pronounced micro-Doppler features, resulting in a wider range of Doppler frequency shifts.

References

[1] Hanif, Ali, et al. "Micro-Doppler based target recognition with radars: A review." IEEE Sensors Journal 22.4 (2022): 2948-2961.

[2] Fang, Xin, and Guoqing Xiao. "Rotor blades micro-Doppler feature analysis and extraction of small unmanned rotorcraft." IEEE Sensors Journal 21.3 (2020): 3592-3601.

[3] Rahman, Samiur, and Duncan A. Robertson. "Classification of drones and birds using convolutional neural networks applied to radar micro-Doppler spectrogram images." IET radar, sonar & navigation 14.5 (2020): 653-661.

[4] Park, Junhyeong, Jun-Sung Park, and Seong-Ook Park. "Small drone classification with light CNN and new micro-Doppler signature extraction method based on A-SPC technique." arxiv preprint arxiv: 2009.14422 (2020).

[5] Gong, Jiangkun, et al. "Detection of micro-doppler signals of drones using radar systems with different radar dwell times." Drones 6.9 (2022): 262

[6] Harmanny, R. I. A., J. J. M. De Wit, and G. Prémel Cabic. "Radar micro-Doppler feature extraction using the spectrogram and the cepstrogram." 2014 11th European Radar Conference. IEEE, 2014.

[7] Jian, Michael, Zhenzhong Lu, and Victor C. Chen. "Experimental study on radar micro-Doppler signatures of unmanned aerial vehicles." 2017 IEEE Radar Conference (RadarConf). IEEE, 2017.

[8] Knott, Eugene F., John F. Schaeffer, and Michael T. Tulley. Radar cross section. SciTech Publishing, 2004.

[9] Borkar, V. G., et al. "Radar cross-section measurement techniques." Defence Science Journal 60.2 (2010): 204.

[10] De Adana, F. Saez, et al. "Method based on physical optics for the computation of the radar cross section including diffraction and double effects of metallic and absorbing bodies modeled with parametric surfaces." IEEE Transactions on Antennas and Propagation 52.12 (2004): 3295-3303.

[11] Chen, Victor C., and W. J. Miceli. "Simulation of ISAR imaging of moving targets." IEE Proceedings-Radar, Sonar and Navigation 148.3 (2001): 160-166.

[12] Chen, Victor C., et al. "Micro-Doppler effect in radar: phenomenon, model, and simulation study." IEEE Transactions on Aerospace and electronic systems 42.1 (2006): 2-21.

[13] Mensa, Dean L. "High resolution radar cross-section imaging." Boston (1991).

[14] Wang, xiaofeng, Chen Wang, and Yuan Liu. "RCS computation and analysis of target using FEKO." Proceedings of 2014 3rd Asia-Pacific Conference on Antennas and Propagation. IEEE, 2014.

[15] Chen, Victor C. The micro-Doppler effect in radar. Artech house, 2019.